Quasiparticle band structures and optical properties of strained monolayer MoS_2 and WS_2

Hongliang Shi,[1] Hui Pan,[1] Yong-Wei Zhang,[1,*] and Boris I. Yakobson[2,†]
[1]*Institute of High Performance Computing, A*STAR, Singapore 138632*
[2]*Department of Mechanical Engineering and Materials Science, Department of Chemistry, and the Smalley Institute for Nanoscale Science and Technology, Rice University, Houston, Texas 77005, USA*
(Received 24 November 2012; revised manuscript received 2 March 2013; published 9 April 2013)

The quasiparticle (QP) band structures of both strainless and strained monolayer MoS_2 are investigated using more accurate many-body perturbation *GW* theory and maximally localized Wannier functions (MLWFs) approach. By solving the Bethe-Salpeter equation (BSE) including excitonic effects on top of the partially self-consistent GW_0 (scGW_0) calculation, the predicted optical gap magnitude is in good agreement with available experimental data. With increasing strain, the exciton binding energy is nearly unchanged, while optical gap is reduced significantly. The scGW_0 and BSE calculations are also performed on monolayer WS_2, similar characteristics are predicted and WS_2 possesses the lightest effective mass at the same strain among monolayers Mo(S,Se) and W(S,Se). Our results also show that the electron effective mass decreases as the tensile strain increases, resulting in an enhanced carrier mobility. The present calculation results suggest a viable route to tune the electronic properties of monolayer transition-metal dichalcogenides (TMDs) using strain engineering for potential applications in high performance electronic devices.

DOI: 10.1103/PhysRevB.87.155304 PACS number(s): 73.22.−f, 71.20.Nr, 71.35.−y

I. INTRODUCTION

Bulk TMDs consisting of two-dimensional (2D) sheets bonded to each other through weak van der Waals forces have been studied extensively owing to their potential applications in photocatalysis[1] and catalysis.[2,3] MoS_2, WS_2, $MoSe_2$, and WSe_2 are examples of such TMDs. Recently, their 2D monolayer counterparts were successfully fabricated using a micromechanical cleavage method.[4] Since then, these monolayer materials have attracted significant attention.[5–12]

For monolayer MoS_2, a strong photoluminescence (PL) peak at about 1.90 eV, together with peaks at about 1.90 and 2.05 eV of the adsorption spectrum, indicated that MoS_2 undergoes an indirect to direct band gap transition when its bulk or multilayers form is replaced by a monolayer.[6–8] Shifts of PL peak for the monolayer MoS_2 were also observed experimentally, which was attributed to the strain introduced by covered oxides.[13] Theoretical studies which employed density functional theory (DFT) method also predicted monolayer MoS_2 to have a direct gap of 1.78 eV.[5] It is known however that DFT does not describe excited state of solids reliably. Furthermore, an important character in low-dimensional systems is their strong exciton binding due to the weak screening compared to bulk cases. Therefore, the good band gap agreement between theoretical and experimental results for monolayer MoS_2 may be a mere coincidence. As a channel material for transistor application, theoretical simulations show that monolayer WS_2 performs better than monolayer MoS_2.[14] In order to address the above questions, it is important and necessary to employ a more accurate calculation method beyond DFT to investigate the electronic structures of strained monolayer MoS_2 and WS_2.

The most common method to circumvent drawback of DFT is the *GW* approximation,[15] in which self-energy operator Σ contains all the electron-electron exchange and correlation effects. The scGW_0 approach, in which only the orbitals and eigenvalues in G are iterated, while W is fixed to the initial DFT W_0, was shown to be more accurate in many cases to predict band gaps of solids.[16] The off-diagonal components of the self-energy Σ should be included in scGW_0 calculations since this inclusion has been proved particularly useful for materials such as NiO and MnO.[17] It is noted that Σ within the *GW* approximation is defined only on a uniform k mesh in the Brillouin zone, due to its nonlocality. Therefore, unlike DFT band structure plot, the QP eigenvalues at arbitrary k points along high symmetry lines cannot be performed directly.[18] Started from the scGW_0 calculation, the QP band structure can be interpolated using the MLWFs approach. This combination was demonstrated to be accurate and efficient for the sc*GW* band structure.[18] The *GW* results were shown to agree well with the photoemission data,[19] while in order to reproduce the experimental adsorption spectra, the consideration of attraction between quasielectron and quasihole (on top of *GW* approximation) by solving BSE is indispensable,[19] particularly for the low-dimensional systems with strong excitonic effect. The main goal of this study is to accurately predict the QP band structures and optical spectra of monolayer MoS_2 as a function of strain by adopting the DFT-scGW_0-BSE approach.

Strain in monolayer MoS_2 can be produced either by epitaxy on a substrate or by mechanical loading. It is well known that strain can be used to tune the electronic properties of materials. This is particularly important for two-dimensional materials, which can sustain a large tensile strain. In fact, shifts of PL peak observed experimentally in monolayer MoS_2 was attributed to strain,[13] and the magnetic properties of MoS_2 nanoribbons could be tuned by applying strain.[20]

By adopting the aforementioned approach, we systematically investigate how the electronic structures and optical properties of monolayer MoS_2 evolve as a function of strain. Our results show that exciton binding energy is insensitive to the strain, while optical band gap becomes smaller as strain increases. Based on the more accurate band structures interpolated by MLWFs methods based on scGW_0 results, the effective masses of carriers are calculated. In addition, this calculation approach is also employed to investigate other monolayer TMDs, that is, WS_2, $MoSe_2$, and WSe_2. Our results demonstrate that the effective mass is decreased as the strain increases, and monolayer WS_2 possesses the lightest carrier

among the TMDs, suggesting that using monolayer WS_2 as a channel material can enhance the carrier mobility and improve the performance of the transistor.

II. DETAILS OF CALCULATION

Our DFT calculations were performed by adopting the generalized gradient approximation (GGA) of PBE functional[21] for the exchange correlation potential and the projector augmented wave (PAW)[22] method as implemented in the Vienna *ab initio* simulation package.[23] Twelve valence electrons are included for both Mo and W pseudopotentials. The electron wave function was expanded in a plane wave basis set with an energy cutoff of 600 eV. A vacuum slab more than 15 Å (periodical length of c is 19 Å) is added in the direction normal to the nanosheet plane. For the Brillouin zone integration, a $12 \times 12 \times 1$ Γ centered Monkhorst-Pack k-point mesh is used. In the following GW QP calculations, both single-shot G_0W_0 and more accurate scGW_0 calculations are performed. 180 empty conduction bands are included. The energy cutoff for the response function is set to be 300 eV, the obtained band gap value is almost identical to the case of 400 eV. The convergence of our calculations has been checked carefully. For the Wannier band structure interpolation, d orbitals of Mo (W) and p orbitals of S (Se) are chosen for initial projections. Our BSE spectrum calculations are carried out on top of scGW_0. The six highest valence bands and the eight lowest conduction bands were included as basis for the excitonic state. BSE was solved using the Tamm-Dancoff approximation. Notice that the applied strain in the present study is all equibiaxial, unless stated otherwise.

III. RESULTS AND DISCUSSIONS

We first analyze the density of states (DOS) for monolayer MoS_2. The d orbitals of Mo and p orbitals of S contribute most to the states around the band gap, similar to previous studies.[9–11] Figure 1 shows the projected d orbitals of Mo and p orbitals of S as well as the decomposed d orbitals for monolayer MoS_2 at the lattice of 3.160 Å (the experimental lattice constant a of bulk MoS_2[9]) and under 3% tensile strain. Based on the DOS, the d orbitals of Mo and p orbitals of S are chosen as the initial projections in the Wannier interpolated method. Figure 2 shows the identical DFT band structures of monolayer MoS_2 obtained by the non-self-consistent calculation at fixed potential and Wannier interpolation method, respectively, confirming that our choice of the initial projections and inner window energy is appropriate. Based on the good results for monolayer MoS_2, the same procedure is also employed for remaining monolayer TMDs.

A. QP band structures of strained monolayer MoS_2

The QP band structures of monolayer MoS_2 at four lattice constants of 3.160, 3.190 (the optimized value from the present work), 3.255, and 3.350 Å are plotted in Fig. 3, corresponding to 0%, 1%, 3%, and 6% tensile strains (with reference to 3.160 Å), respectively. As shown in Fig. 3(a), the band structure obtained by DFT for strainless MoS_2 is a direct band gap semiconductor with a band gap energy of 1.78 eV, while the indirect band gap of 2.49 eV is predicted by G_0W_0. Obviously this G_0W_0 indirect band gap is contrary to the PL observations.[6–8] The QP band structures predicted by our scGW_0 calculation show that MoS_2 is a K to K direct

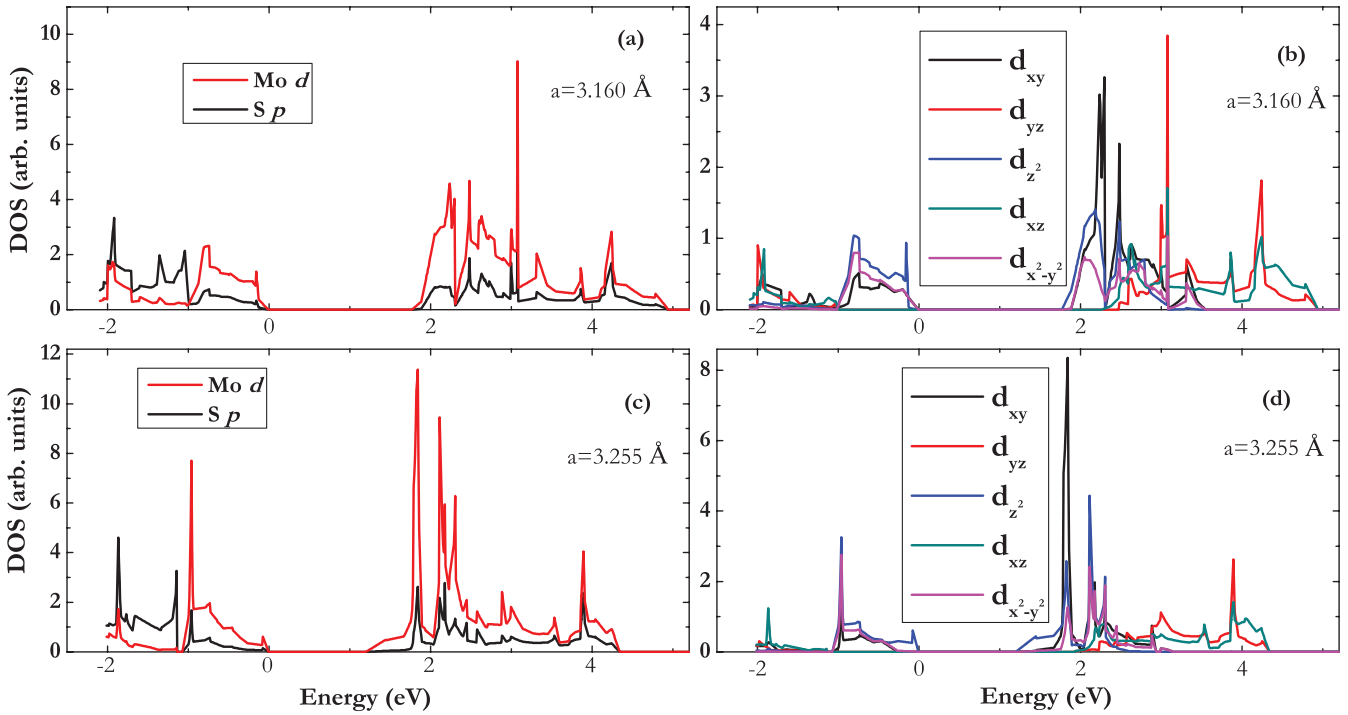

FIG. 1. (Color online) Projected density of states of d orbitals of Mo and p orbitals of S [(a) and (c)] and decomposed d orbital of Mo [(b) and (d)] for monolayer MoS_2 at lattice constants of 3.160 [(a) and (b)] and 3.255 Å [(c) and (d)], respectively. The latter corresponds to 3% tensile strain.

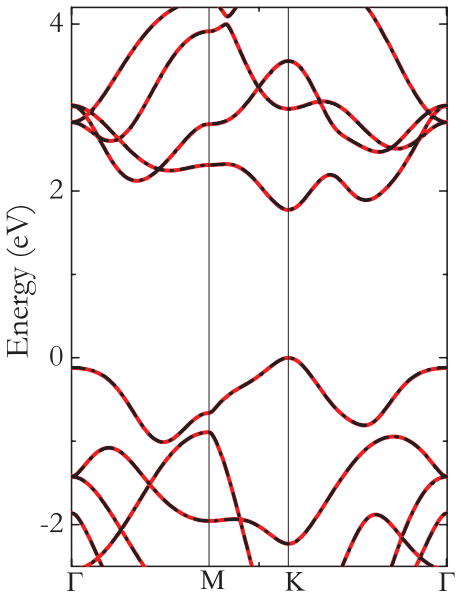

FIG. 2. (Color online) DFT band structures of monolayer MoS_2 at lattice constant of 3.160 Å. Red solid line: Original band structure obtained from a conventional first-principles calculation. Black dash dot: Wannier-interpolated band structure. The Fermi level is set to zero.

band gap semiconductor with a band gap energy of 2.80 eV. This prediction is in excellent agreement with the recent calculation for MoS_2 at the experimental lattice using full-potential linearized muffin-tin-orbital method (FP-LMTO)[24], which predicted a K to K direct band gap of 2.76 eV.

It should be noted that in the 2D materials, the excitonic effect is strong due to the weak screening. Thus it is important to consider the attraction between the quasielectron and quasihole by solving the BSE discussed below in order to make the predicted optical gap consistent with the optical spectra.

Figure 3(b) shows the band structure of monolayer MoS_2 at 3.190 Å corresponding to 1% strain. The DFT result predicts the monolayer MoS_2 to be an indirect band gap with K to Γ of 1.67 eV. Previous DFT studies also found that monolayer MoS_2 already becomes an indirect semiconductor under a tensile strain of 1%.[12] After GW correction, both of the G_0W_0 and scGW_0 QP band structures show that MoS_2 is still a direct semiconductor with K to K band gaps of 2.50 and 2.66 eV, respectively. As the strain increases, shown in Figs. 3(c) and 3(d), the DFT, G_0W_0, and scGW_0 all predict monolayer MoS_2 to be indirect. The calculated indirect band gaps from DFT, G_0W_0, and scGW_0 are 1.20 (0.63), 2.19 (1.56), and 2.23 (1.59) for monolayer MoS_2 under strain of 3% (6%), respectively. As shown in Fig. 3, the value of band gap decreases as the tensile strain increases, accompanying a shift of valence band maximum (VBM) from K to Γ point and resulting in a direct to indirect band gap transition, which was consistent with previous results.[9,12]

The K to K direct and Γ to K indirect band gaps of monolayer MoS_2 obtained by DFT and scGW_0 as a function of tensile strain are plotted in Fig. 4. Clearly our DFT and scGW_0 results have the same trends, and accord well with reported DFT[12] (cyan triangle) and scGW[24] (green solid square) results, respectively. Due to the more accurate description of many-body electron-electron interaction, the scGW_0 band gaps are enlarged about 1 eV compared to DFT results. The optical gap shown in Fig. 4 will be discussed in the next subsection.

B. Excitonic effect in monolayer MoS_2

In this subsection the optical properties of monolayer MoS_2 are discussed in detail. From the technical view, optical transition simulation needs the integration over the irreducible Brillouin zone using sufficiently dense k-point mesh. Naturally the convergence of k-point sampling is important. First, for monolayer MoS_2 at strainless case (3.16 Å), the optical

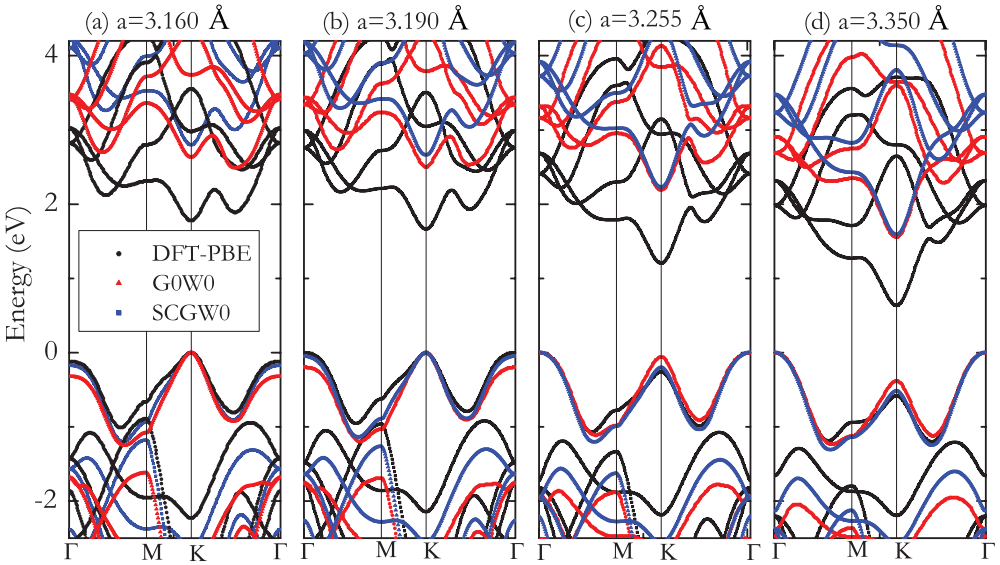

FIG. 3. (Color online) DFT, G_0W_0, and scGW_0 QP band structures for monolayer MoS_2 at lattice constants of (a) 3.160, (b) 3.190 (the optimized lattice constant from this work), (c) 3.255, and (d) 3.350 Å corresponding to 0%, 1%, 3%, and 6% tensile strain (with reference to 3.160 Å), respectively. The Fermi level is set to be zero.

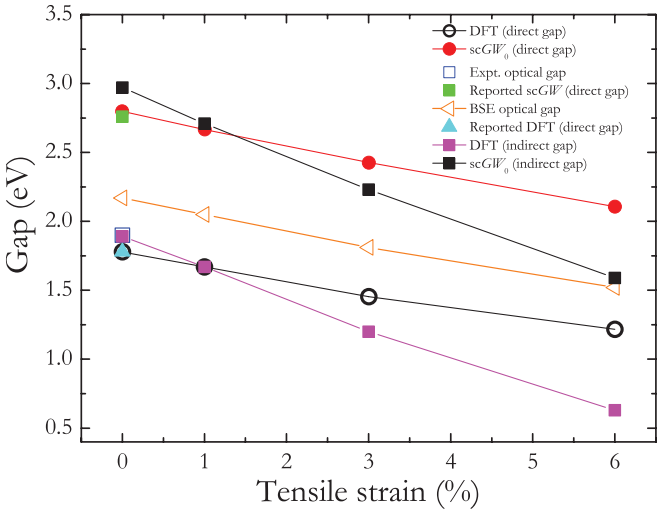

FIG. 4. (Color online) Band gaps for monolayer MoS_2 obtained by DFT, scGW_0, and BSE. Reported experimental (Expt.),[7] DFT,[12] and scGW[24] results are also shown.

adsorption spectra ε_2 ($\varepsilon_{xx} = \varepsilon_{yy}$) obtained by different k-point meshes are illustrated in Fig. 5(a), in which the independent-particle (IP) picture is adopted within DFT (DFT-IP) and no

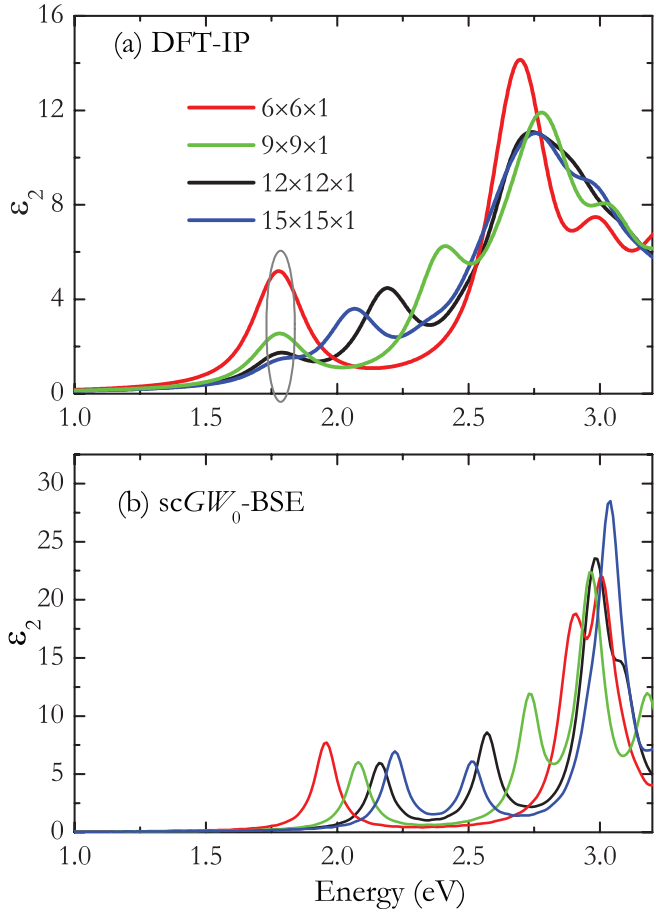

FIG. 5. (Color online) DFT-IP and scGW_0+ BSE adsorption spectra for monolayer MoS_2 at an experimental lattice of 3.160 Å (strainless case) obtained by different k-point meshes.

local filed effect is included at the Hartree or DFT level. The first peak at about 1.78 eV is observed clearly in all the cases, corresponding to the K-K direct transition. The second significant peak located at about 2.75 eV is converged for $12 \times 12 \times 1$ and $15 \times 15 \times 1$ k-point meshes. Other peaks in adsorption spectra between the two aforementioned dominated peaks mainly originate from different irreducible k points with unequal weights in different k-point meshes. According to our analysis of projected density of states, the two significant peaks located at 1.78 and 2.75 eV correspond to d-d and p-d transitions, respectively. Considering the dipolar selection rule only transitions with the difference $\Delta l = \pm 1$ between the angular momentum quantum numbers l are allowed, i.e., the atomic d-d transition is forbidden. However, in the monolayer MoS_2, due to the orbital hybridization, the VBM and conduction band minimum (CBM) still have p orbital contributions, especially the former; thus the VBM to CBM transition dominated by d-d transition is still allowed. As expected, the strength of this d-d transition is weaker than the p-d transition as shown in Fig. 5(a).

As for the BSE calculations, in order to reduce the computational cost, we adopt 400 and 200 eV for the plane wave energy cutoff and response function energy cutoff (short for 400 and 200 eV for energy cutoffs), respectively, while the accuracy still can be guaranteed. Taking the strainless monolayer MoS_2 for example, the scGW_0 band gap is 2.78 eV, resulting in only 0.02 eV difference compared to 2.80 eV aforementioned using 600 and 300 eV for energy cutoffs. The calculated BSE spectra for strainless monolayer MoS_2 are plotted in Fig. 5(b). It is clear that as the k-point mesh refines, the first peaks have a blueshift. For k-point meshes $6 \times 6 \times 1$, $9 \times 9 \times 1$, $12 \times 12 \times 1$, and $15 \times 15 \times 1$, the scGW_0 band gaps are 2.99, 2.84, 2.78, and 2.76 eV, respectively; the first adsorption peaks (optical band gaps) are 1.96, 2.08, 2.16, and 2.22 eV. Correspondingly, the exciton binding energies are 1.03, 0.76, 0.62, and 0.54 eV, inferred from the difference between the QP (scGW_0) and optical (scGW_0-BSE) gaps. These calculated QP band gaps, optical gaps, and exciton binding energies are also listed in Table I. The convergence trend is obvious, particularly for the electronic band gap. However, due to the limitation of computation resource, scGW_0 calculations with more dense k-point mesh are not performed here. Note that previous theoretical results showed a large value of exciton binding energy for monolayer MoS_2. For example, a value of 0.9 eV for monolayer MoS_2 (3.16 Å) was obtained using empirical Mott-Wannier theory;[24] and a value of 1.03 eV was obtained by G_0W_0-BSE calculations for monolayer MoS_2 (3.18 Å) using $6 \times 6 \times 1$ k-point mesh and including spin-orbital coupling,[25] which is the same as our above results using the same k-point mesh without spin-orbital coupling. Binding energy of 0.54 eV reported here is also consistent with 0.5 eV adopting GW and BSE calculations.[26]

Experimentally, two close peaks observed in adsorption spectrum of monolayer MoS_2 around 1.9 eV are due to the valence band splitting caused by spin-orbital coupling. In our calculations, the spin-orbital coupling is omitted unless otherwise stated and this will not alter our main conclusions presented in the current study. In order to make a comparison, we also performed the scGW_0-BSE calculations with spin-orbital coupling using $6 \times 6 \times 1$ k-point mesh

TABLE I. QP band gap, optical band gap, and exciton binding energy for monolayer MoS_2 and WS_2 are obtained by QP scGW_0 and BSE with and without spin-orbital coupling (SOC) adopting different energy cutoffs and k-point mesh. All energies are in the unit of eV.

	Energy cutoffs	k point	E_g	E_g(optical)	Binding energy
Monolayer MoS_2 (3.160 Å)	400 and 200	$6 \times 6 \times 1$(SOC)	2.89	1.87	1.02
		$6 \times 6 \times 1$	2.99	1.96	1.03
		$9 \times 9 \times 1$	2.84	2.08	0.76
		$12 \times 12 \times 1$	2.78	2.16	0.62
		$15 \times 15 \times 1$	2.76	2.22	0.54
	600 and 300	$12 \times 12 \times 1$	2.80	2.17	0.63
Monolayer MoS_2 (3.190 Å)	600 and 300	$12 \times 12 \times 1$	2.66	2.04	0.62
Monolayer WS_2 (3.155 Å)	400 and 200	$6 \times 6 \times 1$(SOC)	3.02	1.97	1.05
		$6 \times 6 \times 1$	3.28	2.21	1.07
		$9 \times 9 \times 1$	3.12	2.34	0.78
		$12 \times 12 \times 1$	3.06	2.43	0.63
		$15 \times 15 \times 1$	3.05	2.51	0.54
	600 and 300	$12 \times 12 \times 1$	3.11	2.46	0.65
Monolayer WS_2 (3.190 Å)	600 and 300	$12 \times 12 \times 1$	2.92	2.28	0.64

and 400 and 200 eV for energy cutoffs. The two peaks in BSE adsorption spectrum located at 1.87 and 2.05 eV and the corresponding exciton binding energy is 1.02 eV, consistent with the aforementioned G_0W_0-BSE calculations using the same k-point mesh and energy cutoffs with different pseudopotentials.[25] Notice that the exciton binding energy obtained with and without spin-orbital coupling for monolayer MoS_2 as shown in Table I is nearly the same, while the optical gap in the former case shifts about 0.1 eV towards lower energy due to the top valence band splitting of 0.17 eV according to our scGW_0 calculation.

For the evolution of exciton binding energy as a function of strain, our results demonstrate that it is almost unchanged, i.e., 0.63 eV (strainless), 0.62 eV (1% strain), 0.62 eV (3% strain), and 0.59 eV (6% strain) (using 600 and 300 eV for energy cutoffs and $12 \times 12 \times 1$ k-point mesh). The direct optical gaps are 2.17, 2.04, 1.81, and 1.52 eV for the four cases shown in Fig. 3, respectively, and also shown in Fig. 4 using the orange left triangles. The experimental optical gap for monolayer MoS_2 was shown to be about 1.90 eV.[7] Since there was no mention of specific lattice parameter, here it is assumed to be the strainless case as shown in Fig. 4. Notice that the consistency is good between our theoretical and experimental results. If spin-orbital coupling is taken into account, the consistency will be improved further since the first peak in the adsorption spectrum moves towards lower energy due to the top valence band splitting. Most importantly, our results demonstrate that the optical gap of monolayer MoS_2 is very sensitive to tensile strain, which can be tuned by depositing monolayer MoS_2 on different substrates,[13] whereas the exciton binding energy is insensitive to it according to our current results. This insensitivity is mainly because the hole and electron are derived from the topmost valence and lowest conduction edge states close to VBM and CBM that are significantly localized on Mo sites (contributed by Mo d orbitals) irrespective of the magnitude of strain according to our DOS analysis.

We also notice that layer-layer distance or the length of vacuum zone implemented in the periodical supercell methods has an important influence on the magnitude of the GW band gap and the exciton binding energy.[27–29] In order to obtain an accurate exciton binding energy, the convergence of k-point mesh, the truncation of Coulomb interaction,[28] and the resulting accurate QP band structure (G_0W_0 or scGW) are necessary. Compared to exciton binding energy of 1.1 eV obtained by interpolation of G_0W_0 band gap,[29] our exciton binding energy obtained using a denser k point is underestimated,[30] due to the finite thickness of vacuum layer adopted in our periodical supercell calculations. However, the magnitude of the optical gap is not affected by the vacuum layer height according to our test (not shown here). An interesting observation is that the optical gap of monolayer MoS_2 is sensitive to the strain while the exciton binding energy is not. Our results also show that the spin-orbital coupling does not change the magnitude of exciton binding energy, while the optical gap reduces towards the experimental result due to the band splitting at K points and better consistency is achieved.

C. Chemical bonding properties of monolayer MoS_2

In order to gain further insight into the electronic structures, we revisit the DOS shown in Fig. 1. For the strainless case, the VBM states at K mainly originate from Mo ($d_{xy} + d_{x^2-y^2}$), and S ($p_x + p_y$) (decomposed p orbitals not shown in Fig. 1). The CBM at K is mainly contributed by Mo d_{z^2} and S ($p_x + p_y$). The Mo d and S p orbitals hybridize significantly, therefore Mo and S form a covalent bond. Bader charge analysis further shows that ionic contribution exists in Mo-S bonds.[31] Notice that MLWFs can also illustrate the chemical bonding properties of solids.[32] The MLWFs shown in Fig. 6 were constructed in two groups. The first group was generated from d guiding functions on Mo. The energy window contains the topmost valence band. Isosurface plots of the Mo d_{xy} MLWFs shown in Fig. 6(a) show d_{xy} orbitals form covalent bonding with $p_x(p_y)$ orbitals and also with a certain ionic component. The second group that MLWFs for the lowest-lying conduction band were also generated from was Mo d guiding functions. Isosurface plots of the Mo d_{z^2} MLWFs shown in Fig. 6(b) show d_{z^2} orbitals form antibonding with $p_x(p_y)$ orbitals. The

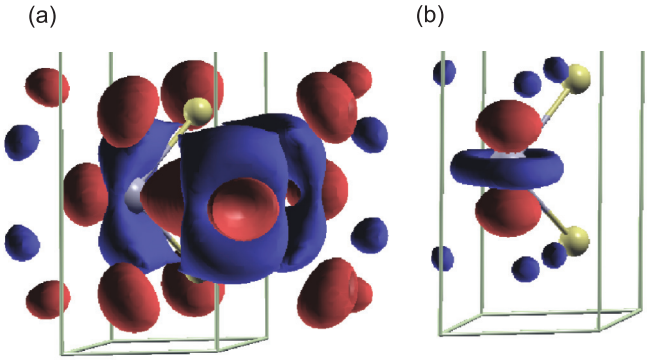

FIG. 6. (Color online) Isosurface plots of (a) valence-band and (b) conduction band MLWFs for MoS_2 (at constant lattice of 3.16 Å), at isosurface values ± 0.9 and $\pm 1.6/\sqrt{V}$, respectively, where V is the unit cell volume, positive value red, and negative value blue. (a) is a Mo d_{xy}-like function showing bonding with the S $p_x(p_y)$ orbital, and (b) is a Mo d_{z^2}-like function showing antibonding with the S $p_x(p_y)$ orbital.

chemical bonding characters demonstrated by MLWFs are consistent with our DOS analysis shown in Fig. 1.

D. QP band structures and optical properties of strained monolayer WS_2

The QP band structures of monolayer WS_2 under tensile strain are also investigated, motivated by its better performance than monolayer MoS_2 used as a channel in transistor devices.[14] The calculation results are illustrated in Fig. 7. Similar to monolayer MoS_2, the scGW_0 QP band structures of monolayer WS_2 also undergo a direct to indirect band gap transition as tensile strain increases. The direct band gaps for the strainless (at the experimental lattice of 3.155 Å[9]) and under 1% tensile strain cases are 3.11 and 2.92 eV, respectively, and the latter corresponds to the optimized lattice constant for monolayer WS_2 from this work. The corresponding indirect band gaps under 3% and 6% tensile strains are 2.49 and 1.78 eV, respectively. Note that for the strainless case, our DFT result predicts monolayer WS_2 to be an indirect band gap semiconductor with CBM only about 16 meV lower than the lowest conduction band at K points, which is contrary to recent full potential methods.[9] The difference may be originated from the technical aspect of these calculations, such as the employed pseudopotential method.[33] However, after the GW correction, a correct direct band gap is achieved.

For optical properties of monolayer WS_2, our calculated QP band gaps, optical gaps, and exciton binding energies are also listed in Table I. It is obvious that the monolayer WS_2 presents many similar properties compared to monolayer MoS_2, for example, the gaps and exciton binding energy also demonstrate a convergence trend as k-point mesh increases; the spin-orbital coupling has little influence on the magnitude of the exciton binding energy. Notice that our scGW_0 calculation predicts the top valence band splitting of monolayer WS_2 to be 0.44 eV, larger than that of monolayer MoS_2 of 0.17 eV, because W is much heavier than Mo. The resulting first peak in BSE adsorption spectrum shifts 0.26 eV towards lower energy, also larger than that of monolayer MoS_2 of 0.1 eV correspondingly. As for the strain effect, the BSE optical gap at our optimized lattice constant of 3.190 Å is 2.28 eV, while at 3.16 Å it is 2.46 eV, as shown in Table I. The former corresponding to 1% tensile strain, results in 0.18 eV reduction of band gaps. This demonstrates that the band gaps and optical gaps are also very sensitive to tensile strain, whereas the exciton binding energy is not. Based on above analysis, we predict the exciton binding energy of monolayer WS_2 is similar to that of MoS_2. Experimentally, the PL maximum of monolayer WS_2 locates between 1.94 and 1.99 eV.[34] Considering the large shift of the peak in the BSE adsorption spectrum caused by spin-orbital coupling, our results at optimized lattice of 3.190 Å are consistent with experimental results.[34,35]

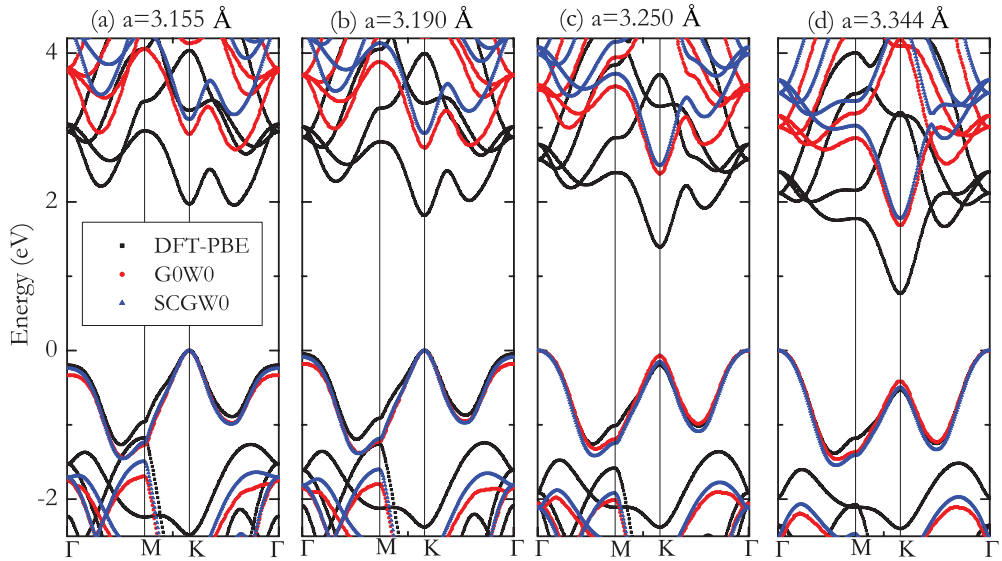

FIG. 7. (Color online) DFT, G_0W_0, and scGW_0 QP band structures for WS_2 at lattice constants of (a) 3.155, (b) 3.190 (optimized lattice constant this work), (c) 3.250, and (d) 3.344 Å , corresponding to 0%, 1%, 3%, and 6% tensile strain (with reference to 3.155 Å), respectively. The Fermi level is set to be zero.

According to our above scGW_0 and BSE calculations for monolayer MoS_2 and WS_2, it is clear that the self energy within the scGW_0 calculations enlarges the band gap by accounting for the many-body electron-electron interactions more accurately, while the strong excitonic effect results in a significant reduction of the band gap. Combining the two opposite effects on band gaps, the final resulting optical gap is consistent with DFT band gaps. Therefore, the good band gap agreement between DFT and experiment is only a coincidence due to the fact that QP band gap correction is almost offset by exciton binding energy. This phenomenon was also observed in hexagonal boron nitride systems, which also have strong excitonic effect.[27,36]

We also perform the scGW_0 QP band structures for monolayer MoS_2 and WS_2 under 1% compressive strains. Our results show that the compressed MoS_2 has a direct band gap of 2.97 eV, while the compressed WS_2 has an indirect band gap of 3.13 eV and K to K direct gap of 3.30 eV.

Our scGW_0 results show that both $MoSe_2$ and WSe_2 are also a direct semiconductor at the strainless state. The experimental lattice constants[9] for $MoSe_2$ and WSe_2 are 3.299 and 3.286 Å and the optimized lattice constants are 3.327 and 3.326 Å, respectively; their direct K-K band gaps are 2.40 and 2.68 eV at experimental lattices and 2.30 and 2.50 eV at the optimized lattices. Compared to the experimental lattice, the optimized lattice corresponds to 0.86% (1.22%) tensile strain for $MoSe_2$ (WSe_2), and the band gap also decreases with increasing tensile strain.

E. Effective mass

Based on the more accurate scGW_0 QP band structures, the effective mass of carriers for TMDs are calculated by fitting the bands to a parabola according to $E = \frac{\hbar^2 k^2}{2 m_e m^*}$, where m_e is the electron static mass. A k-point spacing smaller than 0.03 $Å^{-1}$ is used to keep parabolic effects. Electron and hole effective masses (m^*) at different strains are collected in Table II. For MoS_2 under different strains, the CBM always locates in K point, and the electron effective mass K_e increases with increasing compressive strain while decreases with increasing tensile strain. As for the hole, initially the effective mass also decreases as the tensile strain increases. After the direct to indirect gap transition, VBM shifts to Γ with a heavier hole, which also decreases as the tensile strain increases. Compared to the effective masses of 0.64 and 0.48 for the hole and electron at K point based on DFT calculation performed at the experimental lattice[9] for MoS_2, the effective masses are reduced due to the GW correction in our study.

It is noted that the carrier effective masses obtained by our scGW_0 calculations do not include the spin-orbital coupling effect. Compared with those including spin-orbital effect for monolayer MoS_2,[24] it is found that the electron effective masses are in good agreement while the present hole effective mass is slightly smaller. This is mainly because the spin-orbital coupling alters the curvature of the topmost valence band close to VBM, while the lowest conduction band close to CBM is not affected. The large difference between the scGW (scGW_0) and G_0W_0 result[25] may be due to the poor k-points sampling and non-self-consistent (one-shot) GW calculations of the latter.

For WS_2, $MoSe_2$, and WSe_2, their masses also show similar behaviors. It is noted that at the same strain level, the electron effective mass of WS_2 is the lightest; and electron effective mass decreases as strain increases, making WS_2 more attractive for high performance electronic device applications since a lighter electron effective mass can lead to a higher mobility. Theoretical device simulations also demonstrated that as a channel material, the performance of WS_2 is superior to that of other TMDs.[14]

IV. SUMMARY

In summary, the QP band structures of monolayer MoS_2 and WS_2 at both strainless and strained states have been studied systematically. The scGW_0 calculations are found to be reliable for such calculations. Using this approach, we find they share many similar behaviors. For the optical properties of monolayer MoS_2, exciton binding energy is found to be insensitive to the strain. Our calculated optical band gap is also consistent with experimental results. In addition, we find that the electron effective masses of monolayer MoS_2, WS_2, $MoSe_2$, and WSe_2 decrease as the tensile strain increases, and WS_2 possesses the lightest mass among the four monolayer materials at the same strain. Importantly, the present work

TABLE II. Electron and hole effective masses (m^*) derived from partially scGW_0 QP band structures for monolayer MoS_2, WS_2, $MoSe_2$, and WSe_2 at different strains. The effective masses at K and Γ points are along $K\Gamma$ and $M\Gamma$ directions, respectively.

		Compressive (1%)	Experimental lattices	Optimized lattices	Tensile (3%)	Tensile (6%)
MoS_2	K_e	0.40	0.36 (0.35,[a] 0.60[b])	0.32	0.29	0.27
	K_h	0.40	0.39 (0.44,[a] 0.54[b])	0.37		
	Γ_h				1.36	0.90
WS_2	K_e		0.27	0.24	0.22	0.20
	K_h		0.32	0.31		
	Γ_h				1.24	0.79
$MoSe_2$	K_e		0.38	0.36		
	K_h		0.44	0.42		
WSe_2	K_e		0.29	0.26		
	K_h		0.34	0.33		

[a]Effective masses listed here are averages of the longitudinal and transverse values in Ref. 24.

[b]Effective masses listed here are averages of the curvatures along the ΓK and KM directions in Ref. 25.

highlights a possible avenue to tune the electronic properties of monolayer TMDs using strain engineering for potential applications in high performance electronic devices.

ACKNOWLEDGMENTS

Work at Rice was supported by the U.S. Army Research Office MURI grant W911NF-11-1-0362, and by the Robert Welch Foundation (C-1590).

*zhangyw@ihpc.a-star.edu.sg
†biy@rice.edu

[1] E. Fortin and W. Sears, J. Phys. Chem. Solids **43**, 881 (1982).
[2] W. K. Ho, J. C. Yu, J. Lin, J. G. Yu, and P. S. Li, Langmuir **20**, 5865 (2004).
[3] K. H. Hu, X. G. Hu, and X. J. Sun, Appl. Surf. Sci. **256**, 2517 (2010).
[4] K. S. Novoselov, D. Jiang, F. Schedin, T. J. Booth, V. V. Khotkevich, S. V. Morozov, and A. K. Geim, Proc. Natl. Acad. Sci. USA **102**, 10451 (2005).
[5] S. Lebègue and O. Eriksson, Phys. Rev. B **79**, 115409 (2009).
[6] A. Splendiani, L. Sun, Y. Zhang, T. Li, J. Kim, C. Y. Chim, G. Galli, and F. Wang, Nano Lett. **10**, 1271 (2010).
[7] K. F. Mak, C. Lee, J. Hone, J. Shan, and T. F. Heinz, Phys. Rev. Lett. **105**, 136805 (2010).
[8] T. Korn, S. Heydrich, M. Hirmer, J. Schmutzler, and C. Schüller, Appl. Phys. Lett. **99**, 102109 (2011).
[9] W. S. Yun, S. W. Han, S. C. Hong, I. G. Kim, and J. D. Lee, Phys. Rev. B **85**, 033305 (2012).
[10] P. Johari and V. B. Shenoy, ACS Nano **6**, 5449 (2012).
[11] E. Scalise, M. Houssa, G. Pourtois, V. Afanas'ev, and A. Stesmans, Nano Res. **5**, 43 (2012).
[12] T. Li, Phys. Rev. B **85**, 235407 (2012).
[13] G. Plechinger, F.-X. Schrettenbrunner, J. Eroms, D. Weiss, C. Schuller, and T. Korn, Phys. Status Solidi: Rapid Res. Lett. **6**, 126 (2012).
[14] L. Liu, S. B. Kumar, Y. Ouyang, and J. Guo, IEEE Trans. Electron Devices **58**, 3042 (2011).
[15] L. Hedin, Phys. Rev. **139**, A796 (1965).
[16] M. Shishkin and G. Kresse, Phys. Rev. B **75**, 235102 (2007).
[17] S. V. Faleev, M. van Schilfgaarde, and T. Kotani, Phys. Rev. Lett. **93**, 126406 (2004).
[18] D. R. Hamann and D. Vanderbilt, Phys. Rev. B **79**, 045109 (2009).
[19] G. Onida, L. Reining, and A. Rubio, Rev. Mod. Phys. **74**, 601 (2002).
[20] H. Pan and Y.-W. Zhang, J. Phys. Chem. C **116**, 11752 (2012).
[21] J. P. Perdew, K. Burke, and M. Ernzerhof, Phys. Rev. Lett. **77**, 3865 (1996).
[22] G. Kresse and D. Joubert, Phys. Rev. B **59**, 1758 (1999).
[23] G. Kresse and J. Furthmüller, Phys. Rev. B **54**, 11169 (1996).
[24] T. Cheiwchanchamnangij and W. R. L. Lambrecht, Phys. Rev. B **85**, 205302 (2012).
[25] A. Ramasubramaniam, Phys. Rev. B **86**, 115409 (2012).
[26] J. Feng, X. Qian, C.-W. Huang, and J. Li, Nat. Photonics **6**, 866 (2012).
[27] L. Wirtz, A. Marini, and A. Rubio, Phys. Rev. Lett. **96**, 126104 (2006).
[28] C. A. Rozzi, D. Varsano, A. Marini, E. K. U. Gross, and A. Rubio, Phys. Rev. B **73**, 205119 (2006).
[29] H.-P. Komsa and A. V. Krasheninnikov, Phys. Rev. B **86**, 241201(R) (2012).
[30] We get the interpolated band gap of 3.18 eV for monolayer MoS_2 at 3.16 Å using using 400 and 200 eV for energy cutoffs and 12 × 12 × 1 k-point mesh following the methods in Ref. 29. Considering our results that optical gaps are not affected by the thickness of vacuum layer, the exciton binding energy is about 1.02 eV, consistent with conclusions in Ref. 29.
[31] Q. Yue, J. Kang, Z. Shao, X. Zhang, S. Chang, G. Wang, S. Qin, and J. Li, Phys. Lett. A **376**, 1166 (2012).
[32] F. Freimuth, Y. Mokrousov, D. Wortmann, S. Heinze, and S. Blügel, Phys. Rev. B **78**, 035120 (2008).
[33] We also test the recently released pseudopotential by employing 14 valence electrons instead of the 12 current ones for W in the DFT calculations, the direct band gap of 1.95 eV for monolayer WS_2 at 3.155 Å is obtained with CBM, 21 meV lower than the local minimum at about the middle point along K to Γ, similar to the results obtained by the full potential method in Ref. 9. The resulted scGW_0 QP band structures of monolayer WS_2 are also similar to that presented in Fig. 7, and the main conclusions for monlayer WS_2 remain unchanged.
[34] H. R. Gutiérrez, N. Perea-López, A. L. Elias, A. Berkdemir, B. Wang, R. Lv, F. López-Urias, V. H. Crespi, H. Terrones, and M. Terrones, Nano Lett., doi: 10.1021/nl3026357.
[35] W. Zhao, Z. Ghorannevis, L. Chu, M. Toh, Ch. Kloc, P.-H. Tan, and G. Eda, ACS Nano **7**, 791 (2013).
[36] M. Bernardi, M. Palummo, and J. C. Grossman, Phys. Rev. Lett. **108**, 226805 (2012).